DEGREE PROJECT IN MECHANICAL ENGINEERING,
SECOND CYCLE, 30 CREDITS
STOCKHOLM, SWEDEN 2018

Influence of loading on bone growth at the growth plates in immature rat metatarsals

MOFYA MAINDA, PHILIP WERNSTEDT

KTH ROYAL INSTITUTE OF TECHNOLOGY
SCHOOL OF ENGINEERING SCIENCES

Influence of loading on bone growth at the growth plates in immature rat metatarsals

MOFYA MAINDA, PHILIP WERNSTEDT

Date: June 4, 2018
Supervisor: Elena Gutierrez Farewik
Co-supervisor: Farasat Zaman
Examiner: Elena Gutierrez Farewik
KTH Royal Institute of Technology Department of Mechanics
SE-100 44 Stockholm, Sweden

Acknowledgement

We would like to express a special thanks to our supervisor Elena Gutierrez Farewik for her support and guidance during this study.

A special thanks to our co-supervisor Farasat Zaman for his guidance and support during the experimental study.

We would also like to thank the teaching staff at the Solid Mechanics department at KTH for their support and knowledge that helped complete this thesis.

The authors thank the Swedish Institute for their support.

Abstract

Growth of different bones in children is facilitated by different mechanisms according to the anatomical site and function of the bone. Longitudinal bone formation in long and short bones occurs in the cartilaginous growth plates located at each end of the growing bone through a process known as endochondral ossification. This growth continues until a child becomes full-grown at which point the growth plate calcifies to solid bone [1]. It is still unclear how mechanical and biological factors affect bone growth. For the purpose of this study, immature rat metatarsals have been subjected to varying number of cycles (1, 5, 10 and 50 cycles) in order to better understand the effect that mechanical loading has on bone growth. This has been done using two consecutive trials. The trends in these trials were analyzed and compared. Specimens subjected to 5 cycles exhibited the most prominent effect of loading over the course of 16 days. The results of the trials reveal that immature bones are sensitive to cyclic compressive loading. The results revealed a potential threshold below which the loading resulted in an increased growth. Furthermore, simulations of longitudinal bone growth using a thermal-structural coupled analysis, with the findings from the experiment, has been performed. The model results in a stress free structure that is comparable to the growth of the experiments to a certain extent. The model also allowed incorporation of the bent growth that is observed in the experiments.

Table of Contents

1 Introduction

Bone disorders in children can be a result of different causes such as cancer or injury. They may get worse or better as the child grows and in most cases the cause of these born deformities is unknown. Children born with bone deformities may experience severe pain, disability and discomfort that often make physical activities difficult. A case of bone deformities that manifest in infancy and childhood are hypophosphatemic rickets (HPR) which denotes a group of metabolic bone diseases with common biochemical, biomechanical, and clinical features. Abnormal mineralization of growth cartilage and in newly formed bone collagen induces various deformities commonly found around the knee [2].

Traditional pharmacological treatment options of some orthopedic deformities mainly aim to supplement mineral deficiencies but do not help the obvious physical deformities which may be a result of widening growth plates for example. As a result, most children require corrective surgery or the implementation of various fixation devices such as Ilizarov devices and Kirschner wires. These current fixation devices are uncomfortable and may be a source of anxiety for patients because they are very noticeable and make it difficult for the children to interact with their peers [2]

Growth of different bones in children is facilitated by different mechanisms according to the anatomical site and function of the bone. Longitudinal bone formation in long and short bones occurs in the cartilaginous growth plates located at each end of the growing bone through a process known as *endochondral ossification*. This growth continues until a child becomes full-grown at which point the growth plate calcifies to solid bone [1].

There are many mechanical and biological factors that contribute to endochondral ossification. Although previous studies have attempted to investigate the influence of different mechanical loading on both mature and immature bones, there is still much to be understood about the growth plate mechanism that is responsible for bone growth from infancy to adolescence. Furthermore, it is still unclear how mechanical factors influence bone growth in children.

2 Background

2.1 Structure of Bone

A young bone consists of important parts that can be distinguished from each other. The extremities of the bone are where the *epiphyses* are found (one at each end). The elongated shaft of the bone, known as the diaphysis makes up most of the length of the bone. Both the epiphyses and diaphysis ossify from an independent center. The ends of diaphysis near the epiphyses are known as *metaphyses* [3]. Each metaphysis is the zone of active growth of a long bone. The metaphyses are richly supplied with blood through end arteries forming hair pin bends. This is the common site of osteomyelitis in children [4]. The metaphyses and epiphyses are separated by cartilaginous *growth plates*. Figure 1 is a schematic illustration of the microscopic structure of a typical long bone.

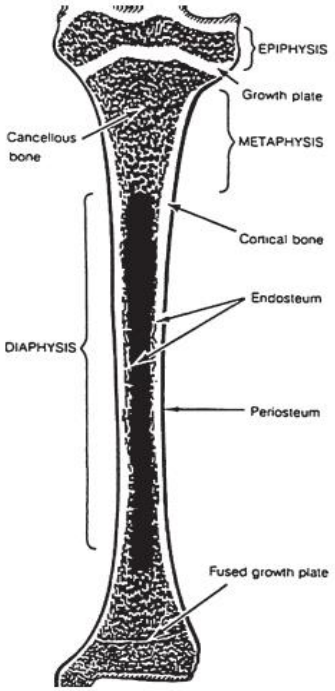

Figure 1: Schematic structure of a tibia (long bone) showing the proximal epiphysis, middle diaphysis, fused distal growth plate, active proximal growth plate and the metaphysis [3]

2.2 Growth Plates

The growth plates are located at the ends of the bone, i.e. one at each end of the bone. It is a plate of cartilage separating epiphyses from metaphyses. The cells of this cartilage plate multiply and grow in size thereby elongating the length of the bones. When the age of maturity arrives, this cartilage plate ossifies at which point the bone can no longer grow in length. This plate of cartilage is nourished by both epiphyseal and metaphyseal arteries.

The growth plate is avascular, aneural and consists of chondrocytes embedded in an abundant extracellular matrix. In most species, the non-ossified growth plate disappears at skeletal maturity, although some species such as the rat retain an essentially inactive growth cartilage [1].

A section of a growth plate reveals ordered columns of chondrocytes that are smaller and more flat at the top (epiphyseal end) and become larger and rounder towards the metaphysis. There is a highly ordered differentiation of these chondrocytes into three distinct zones, the reserve, proliferative and hypertrophic zones. The relative proportions of the three zones vary from species to species [5]. Figure 2 and Figure 3 show the structure and histology of the growth plates.

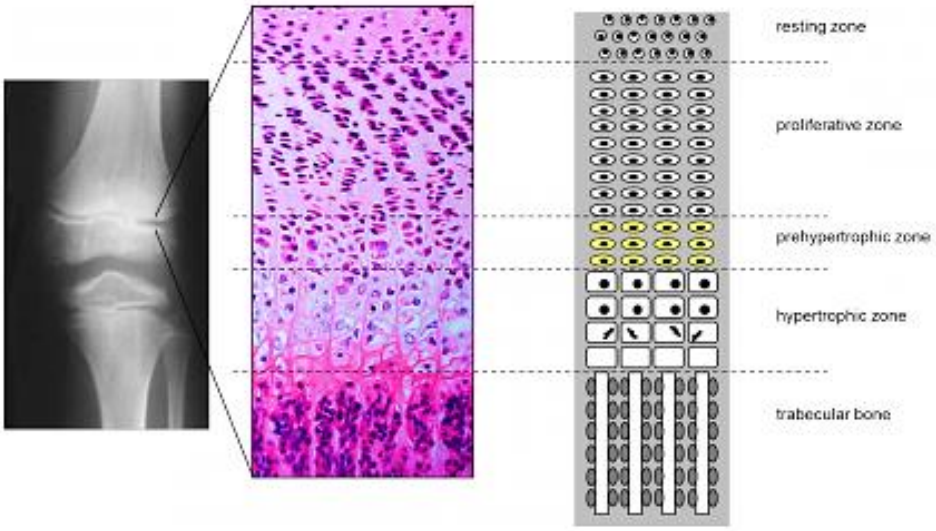

Figure 2: Growth plate zones [6]

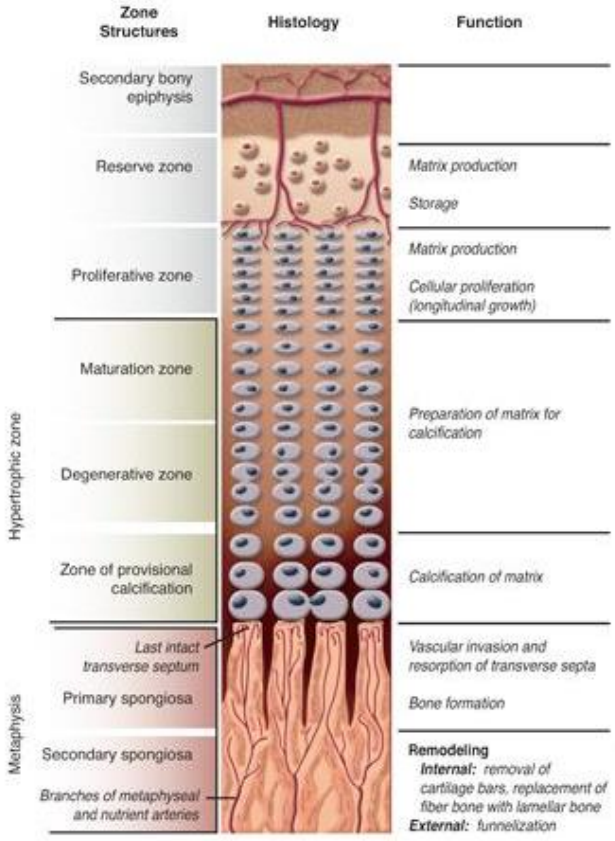

Figure 3: Growth plate zones histology and function [7]

2.3 Longitudinal Bone growth

Long, short and flat bones grow longitudinally by the process of endochondral ossification. Each of the bones is pre-formed as a hyaline cartilage model. Bone tissue is then deposited beginning in the middle of the model on the calcified cartilaginous core using the endochondral ossification mechanism. During endochondral ossification, chondrocytes proliferate, undergo hypertrophy and die; the cartilage extracellular matrix they construct is then invaded by blood vessels, osteoclasts, bone marrow cells and osteoblasts, the last of which deposit bone on remnants of cartilage matrix. As blood vessels, osteoclasts, and osteocytes continue to invade, the bone shaft (diaphysis) will start to lengthen. As a result the medullary cavity (hollow inner cavity) is formed and the diaphysis will slowly continue

to increase in length during prenatal development. With time, the amount of cartilage in the tissue becomes less as the percentage of bone and the extent of its mineralization increases [1].

Endochondral ossification requires the presence of a hyaline cartilage. Early in gestation, mesenchymal precursor cells aggregate to form models of the future long bones. A cartilage model develops, and the peripheral cells organize into a perichondrium [1]. Chondrocytes (cartilage cells) expand and degenerate, and the matrix surrounding them calcifies. This calcification begins in the center of the diaphysis and becomes the primary ossification center. Vascular buds enter the ossification center and transport new mesenchymal cells capable of differentiating into osteoblasts, chondroclasts, and osteoclasts. These cells align themselves on the calcified cartilage and deposit bone. Primary cancellous bone is thus formed, and ossification expands toward the metaphyseal regions.

2.4 Factors affecting bone growth

Bone growth is influenced by two main factors: *biological* and *mechanical*. The biological factors are regulated by nutrition, genetics and hormones [5]. The mechanical factors results from the force acting on the bone, which mainly depends on a level of physical activity (walking, running, etc) during a child's daily routine.

The effects of mechanical stimuli on bone growth have been debated and investigated over an extensive time period. As early as 1892, Wolff presented the well-known, Wolff's law for bone adaptation [8]. Many other scientists have since contributed and/or improved on this law.

Thompson stated that "a condition of strain, the result of stress, is a direct stimulus to growth itself" [9]. Frost added to Thompson's theory by pointing out that a minimum effective strain threshold needs to be surpassed before bone adaptation would occur [10]. In 1971, Hart et al. performed experiments on rabbits and came to the conclusion that it was dynamic and not static loading that increased the bone growth [11]. The fact that dynamic loading is a key component for bone growth has later been confirmed by several researchers [12], [13]. The latter also showed that the frequency of the loading waveform is an important factor for bone adaptation. Turner summarized the previous findings and performed confirmatory experiments and came up with the conclusion that "a) dynamic strains drive bone adaptation; (b) the strain stimulus is increased if the magnitude or frequency of the dynamic signal is increased; and (c) increasing strain rate enhances the strain stimulus." [14]

In contrast to Wolff's law, the Hueter–Volkmann law states that increased pressure on the plates retards bone growth and, conversely, reduced pressure or tension accelerates it. The two laws are not strictly contradictory, but highlight the complexity and incomplete knowledge of bone growth. This was further endorsed by Frost that proposed that for stresses not exceeding a certain physiological range, endochondral bone growth speeds up in the case of compression compared to tension. Compression exceeding the physiological range slows down or even inhibits growth meaning that there is a threshold for when compression loading switches from inhibiting to aiding bone growth [10].

In the recent years, several studies have investigated the effects of both static loading [15], [16] and dynamic loading [15], [16], [17], [18], [19], [20], [21] on the growth rate of bone and cartilage. It has been reported that compressive loading inhibits growth rate and the height of the growth plate [15], [16], [18]. Ménard et al. investigated and compared the effects of both static and dynamic compressive loading in a series of experiments on rats. The results showed that compressive loading (static and dynamic) initially reduced the growth rate and growth plate height significantly compared to non-loaded specimens. However, continuing the experiment over a longer time period the results between the groups started to level out. Additionally, growth resumption was observed after loading removal for both statically and dynamically loaded specimen [16].

Maeda et al. preformed studies on immature chick bones in order to investigate the effects of cyclic compression on the calcification process. In contrast to previously mentioned findings, Maeda et al. reported that the loading resulted in growth of bone matrix similar that of natural maturation.

Furthermore, cyclic compressive loading was suggested to enhance bone calcification which in turn significantly increased the elastic moduli in that area. No significant changes in moduli were observed in the control group [22].

A review of the literature presents two challenges; 1. The mechanisms and factors affecting bone growth are not fully understood. 2. Most studies focus on the remodeling of bone or bone growth of mature bone. How mechanical stimuli influence immature bone or bone under development is still a relatively unexplored area. Additionally, most studies use a predefined cyclic loading for all test specimens or only make variations in the amplitude of the loading. In order to investigate the full effects of cyclic loading, additional variation of said loading must be performed.

The aim of this thesis was to study how varying the number of cycles of cyclic compressive loading can affect the bone growth in order to better understand the mechanical factors contributing to bone growth. It is hypothesized that there is a direct correlation between the number of cycles of cyclic compression and bone growth rate. This understanding of early bone development can be helpful in devising treatment for bone deformities.

Additionally, the aim was to create a finite element model to simulate biological bone growth without the addition of external loads.

3 Materials and Methods

3.1 Metatarsal bone organ culture system

The three middle metatarsal bones were dissected from the back paws of fetal Sprague-Dawley rats (19–20 days p.c.). The pregnant rats were sacrificed using CO_2 asphyxiation. There were two consecutive trials conducted for the study. For the initial trial, 17 metatarsals bones were extracted and 20 metatarsals were later extracted for the second trial. The dissection media contained 1xPBS with Fungizone (2.5 μg/ml), penicillin (100 U/ml), and streptomycin (100 μg/ml; all purchased from Invitrogen. Each bone was transferred to a separate well in 24-well plates with 0.4 ml/well of MEM with l-glutamine (Invitrogen), supplemented with 0.05 mg/ml ascorbic acid (Apoteksbolaget, Göteborg, Sweden), 1 mM sodium glycerophosphate (Sigma), 0.2% bovine serum albumin (BSA; Sigma), 100 U/ml penicillin, and 100 μg/ml streptomycin. The metatarsals bones used in trial one were cultured for 5 days and the bones used for trial two were cultured for 6 days. The bones were kept at 37°C with 5% CO_2 and cell culture medium was changed on every 2-3 days. The bones extracted were from animals sacrificed for other projects approved by the ethical committee at Karolinska Institutet.

3.2 Mechanical testing and Measurement of longitudinal growth

The specimens were loaded using ADMET Materials Testing Machine and the data was analyzed with MTESTQuattro (ADMET, Norwood, MA). One end of the bone was constrained in a retrofitted holder and a piston was applying the axial pressure at the free growth plate. An aerial view of the setup is shown in Figure 4. The piston was displacement controlled at 0.01 mm/s up to a predefined maximum load of 0.05 N. After reaching the maximum load, the bones were immediately unloaded. The loading sequence was carried out with varied amount of cycles. Upon analysis of the trial 1 measurement data collected on day nine, trial 2 was initiated with a modified protocol. The control bones were subjected to the same treatment as the test specimens with the exception of the longitudinal loading. They were loaded into the retrofitted holder for the same amount of time as the testing procedure lasted thus being extracted from the culture media during that time. In the first trial, one control bone was assigned to a specified number of cycles (i.e. 1, 5, 10, and 50) since different amount of cycles implies a different total testing time for the procedure. In the second trial, the described protocol for the control group was changed since the difference in time between different groups was negligible. The control bones in the second trial were chosen due to their shape not being suitable for longitudinal loading. Figure 5 lists the protocol for each bone and Figure 6 shows how the bone was placed in the retrofitted holder. Figure 28 and Figure 29 in Appendix A shows examples of loading cycles for two different specimens.

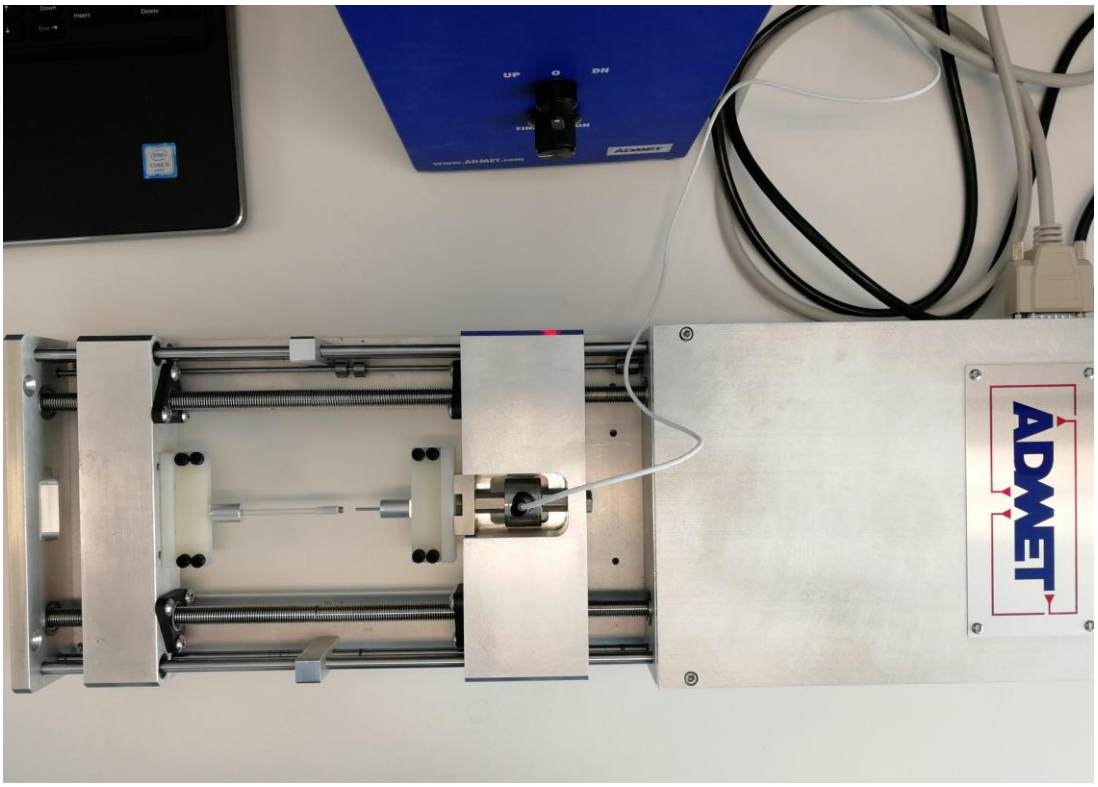

Figure 4: Aerial view of the experimental setup

Trial 1
Test specimen 1
Test specimen 2
Test specimen 3
Test specimen 4
Test specimen 5
Test specimen 6
Test specimen 7
Test specimen 8
Test specimen 9
Test specimen 10
Test specimen 11
Test specimen 12
Test specimen 13
Test specimen 14
Test specimen 15
Test specimen 16
Test specimen 17

Trial 2
Test specimen 1
Test specimen 2
Test specimen 3
Test specimen 4
Test specimen 5
Test specimen 6
Test specimen 7
Test specimen 8
Test specimen 9
Test specimen 10
Test specimen 11
Test specimen 12
Test specimen 13
Test specimen 14
Test specimen 15
Test specimen 16
Test specimen 17
Test specimen 18
Test specimen 19
Test specimen 20

Color legend
Control group
Number of cycles: 1
Number of cycles: 5
Number of cycles: 10
Number of cycles: 50

For all test specimens:

Maximum amplitude: 0.05 N

Displacement control: 0.01 mm/s

Figure 5: Testing protocol including color legend for trials 1 and 2

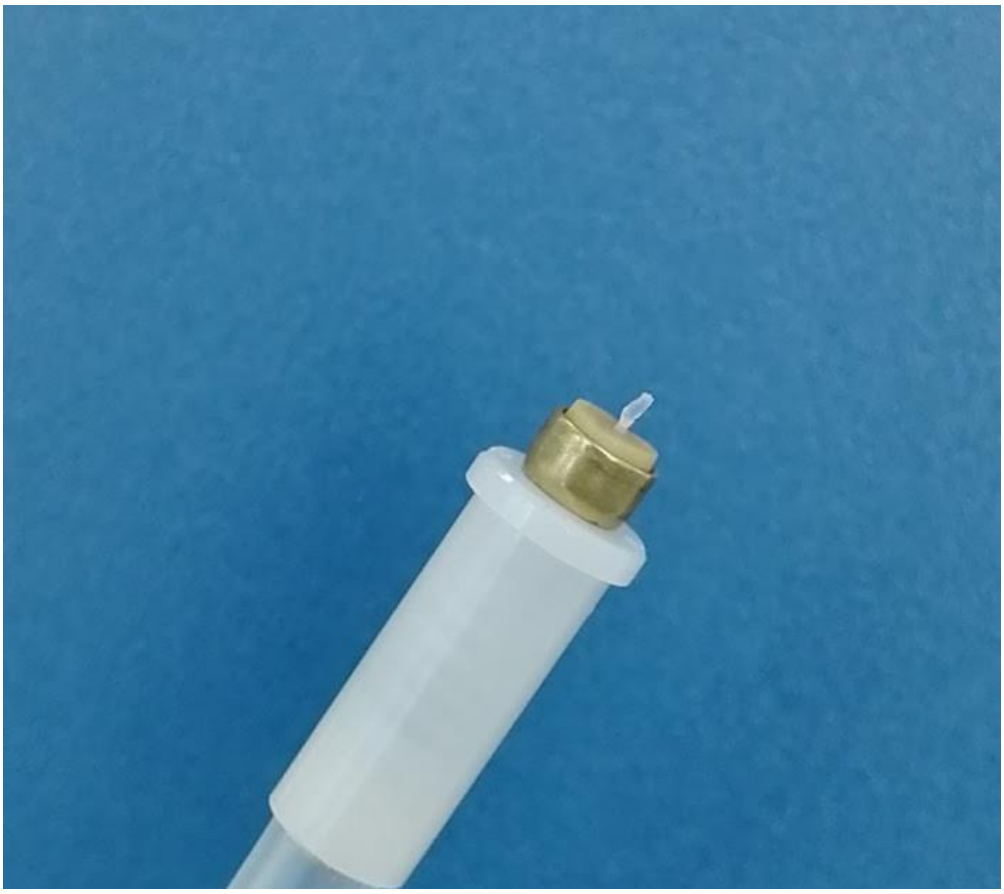

Figure 6: Metatarsal bone placed in the retrofitted holder

Digital pictures were taken of each metatarsal bone with 1.5x magnification at days 0, 2, 4, 7, 9, 11 and 16 for the first trial of culture and at days 0, 2, 4, 7, 9, 14 and 16 for trial 2, using Infinity digital camera attached to a Nikon SMZ-U microscope. Next, the longitudinal growth of the metatarsals was measured using the Infinity-image analysis system (built in camera). Both the total length of each bone as well as the increase expressed as a percentage of the initial length were analyzed. Due to human error, the first registered lengths (i.e. day 0) in trial 1 were lost during the analysis, leading to day two serving as baseline only for the first trial.

4 Modelling

4.1 Theory

As previously stated, bone growth at the growth plates is a process by which columnar chondrocytes proliferate, hypertrophy and then mineralize into calcified bone thereby increasing the length of the bone.

In order to model the bone growth without applied forces, a temperature incremental approach was used. An initial calcification temperature was assigned to the lower boundary of the model which represented the calcified zone (trabecula bone). It was theorized that the cartilage would gradually expand in the longitudinal direction with an increase in temperature until the calcification temperature was reached. Once that temperature was reached, the cartilage was turned into bone (adopting all the assigned material properties of bone) and the expansion stopped at that point. In order for the expansion to stop, a step function was created to determine the secant coefficient of thermal expansion. The coefficient was set so as to allow expansion only in the longitudinal direction. At the calcification temperature, with the use of the step function, the thermal expansion coefficient was set to zero, resulting in termination of expansion. This thermal expansion reflects the physiological growth of longitudinal bone growth. The step function used to compute thermal expansion is shown in Figure 7.

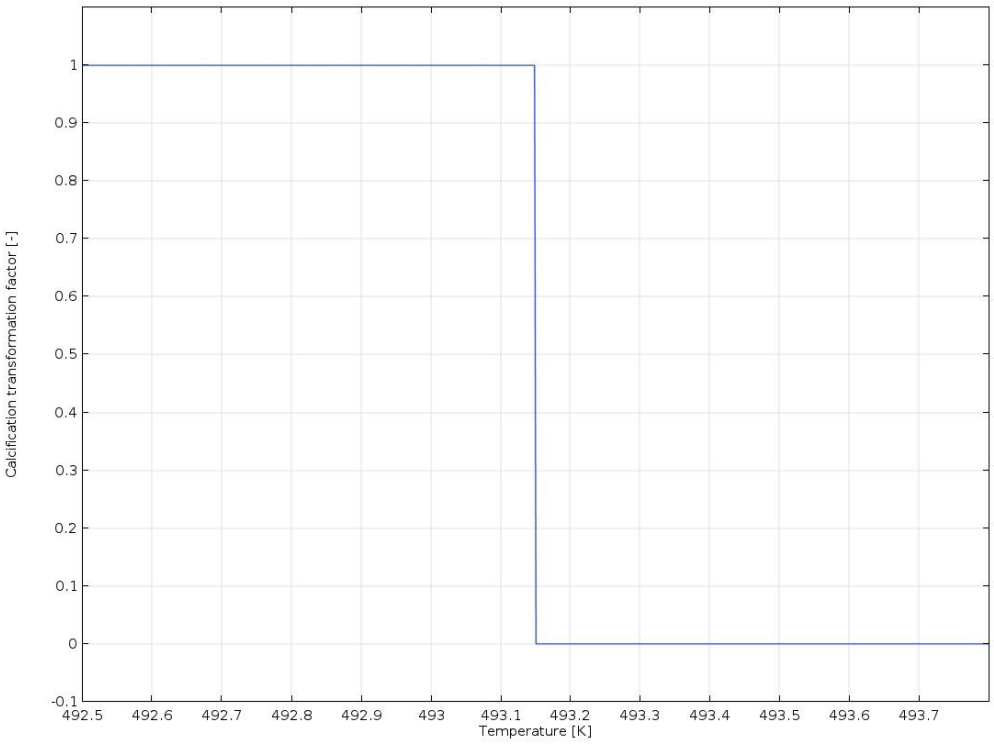

Figure 7: Step function used to calculate thermal expansion change as a function of Temperature

The Young's modulus was changed according to the linear relationship shown in Figure 8, thereby adopting the assigned properties of bone with change in temperature. The thermal properties required to carry out a thermal analysis were arbitrary chosen in order to obtain a temperature field that satisfied the criterion.

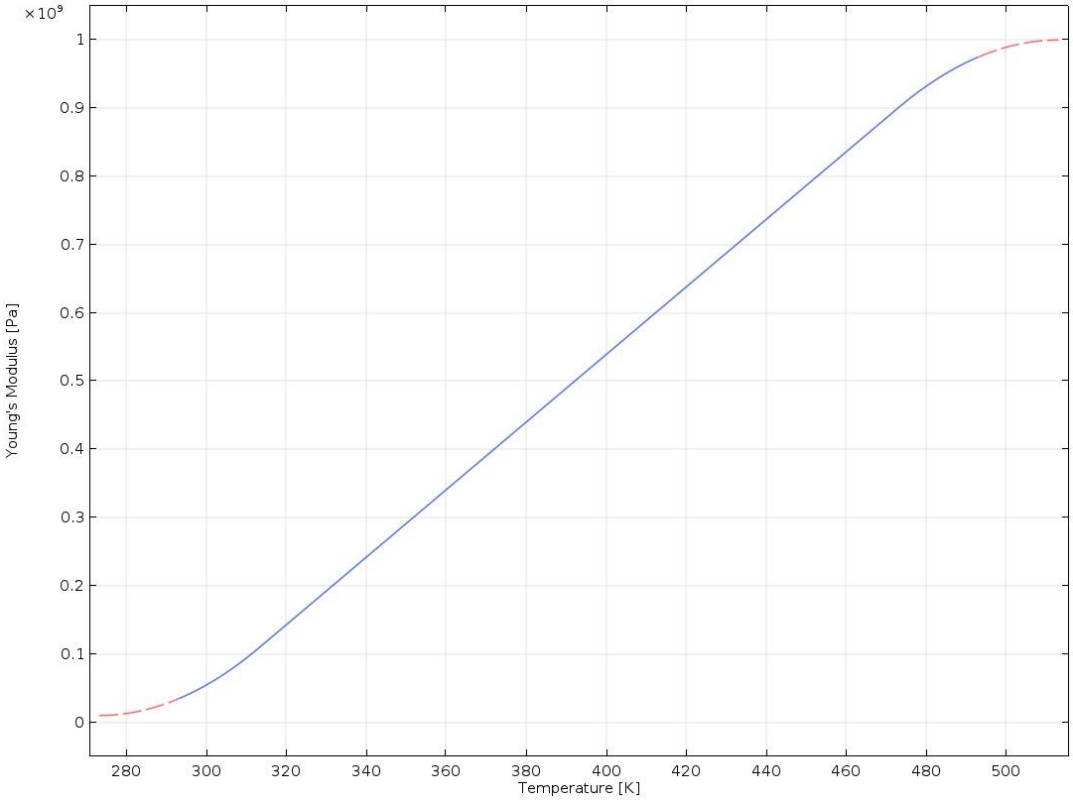

Figure 8: Linear function of Young's Modulus as a function of Temperature

A thermo-mechanical analysis was then performed to model/investigate the effects of the thermal expansion on the elongation and stresses. Figure 9 illustrates the steps that were taken to compute the bone growth as a result of the temperature change. For load case 1, a time range of 1200 s was set in order to allow for the heat transmission through the majority of the body. Due to computational time, the time range for load case 2 was reduced to 400 s.

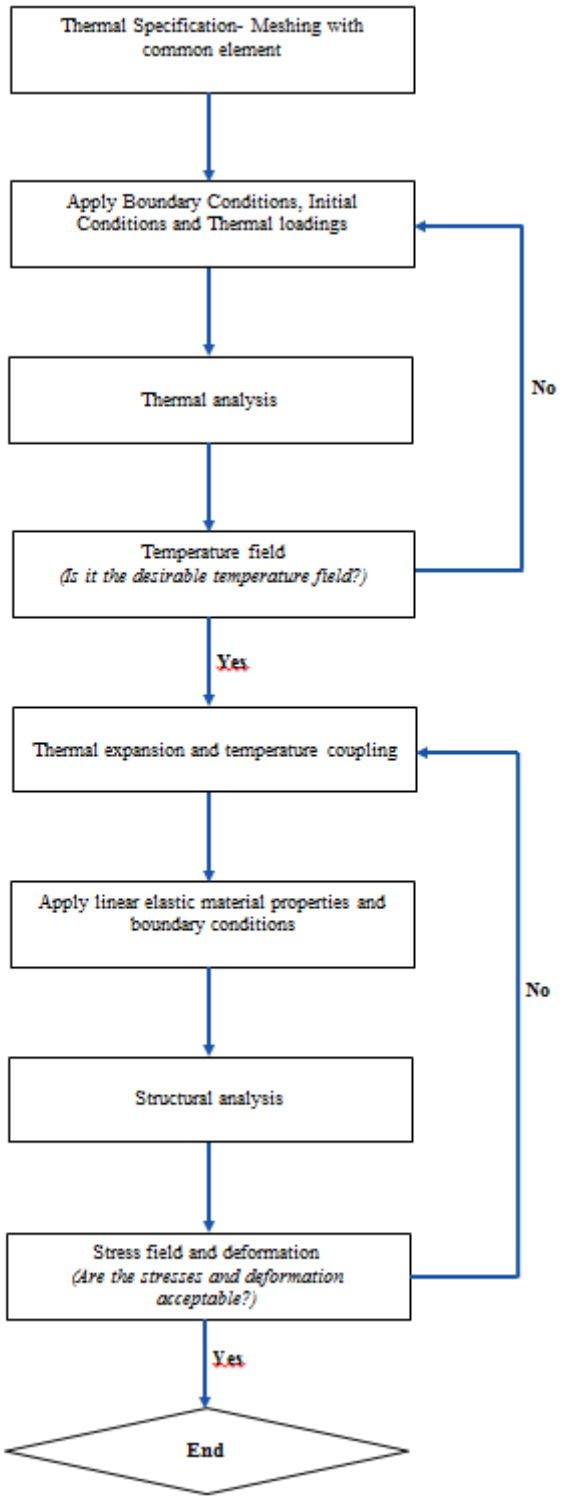

Figure 9: Flow chart of analysis used to compute the bone growth as a function of temperature

4.2 Geometry and material properties

The cartilaginous growth zone was modelled as a hollow cylinder with inner radius 0.15 mm, outer radius 0.25 mm and length 1 mm in COMSOL Multiphysics® (COMSOL AB, Stockholm). Bone and cartilage were treated as linear isotropic materials. For simplification, the growth plate was modelled as one growth zone with the same Young's modulus and Poisson's ratio as opposed to sectioning it according to the different zones. The geometry was layered in order to apply different load cases of temperature. A sweeping mesh with quadrilateral face meshing method was used. For the face along

the z-axis a coarser predefined size was applied. For the faces at the ends of the cylinder, the minimum element size was set to 0.018 mm, the maximum element size was set to 0.08 mm and the curvature factor was set to 0.372. A total of 7080 degrees of freedom was solved for. The completed mesh is shown in Figure 10 and the mechanical properties are summarized in Table 1.

Table 1: Material properties used in the computational model

Material parameters	**Cartilage**	**Calcified bone**
Young's Modulus, E [MPa] [23]	10	1000
Poisson's ratio, $\boldsymbol{\nu}$ [-] [23]	0.167	0.27
Thermal conductivity, K [$W \cdot m^{-1} \cdot K^{-1}$]	1.25e-7	1.25e-7
Specific heat, Cp [J/(kg·K)]	10	10
Density, ρ [kg/m^3]	100	100
Thermal expansion coefficient α [1/K]	0.005	0

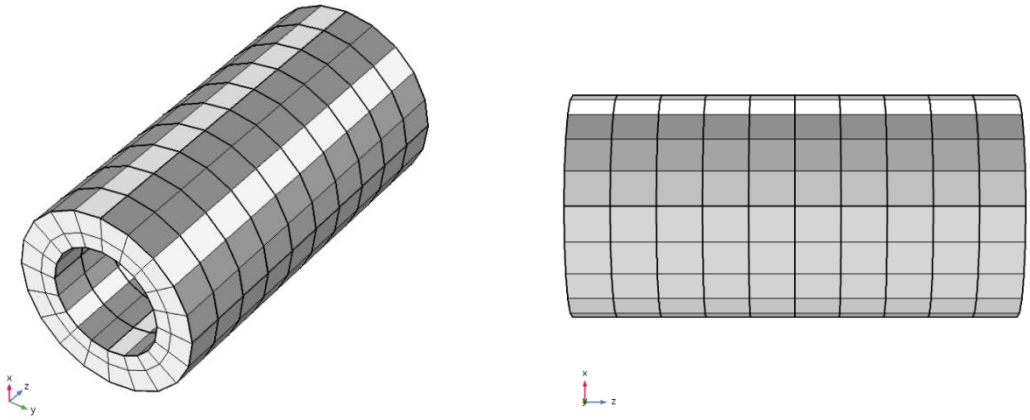

Figure 10: The Finite element model with quadrilateral elements implemented in COMSOL

4.3 Boundary Conditions

Two load cases were considered for the computational model. For load case 1, the calcification temperature was applied on the lower boundary. For load case 2, the calcification temperature was applied on selected layers of the geometry. Thermal insulation was applied to the remaining boundaries. A fixed constraint was also applied on the entire lower boundary for both load cases. This was the demarcation between the calcified bone and the growth zone. An initial value of 293.15 K was assigned to the geometry.

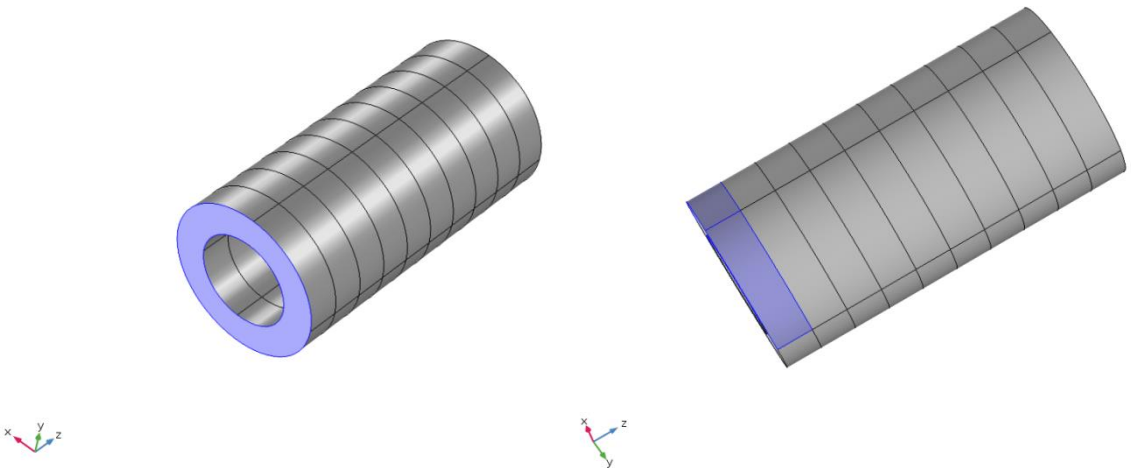

Figure 11: Temperature load cases analyzed in the model. Load case 1: Temperature applied on entire lower boundary (left figure). Load case 2: Temperature applied on selected layers (right figure).

5 Results

5.1 Experimental Results

5.1.1 Trial 1

The results of percentage length at each day of measurement were compiled and plotted in Figure 12-Figure 15 and compared with the arithmetic mean of control bones.

Specimens #2 and #5 were damaged and fractured during manual handling therefore were discarded from the analysis. The results show that the control bones had a larger growth rate during the early stages of growth (day 2-day 4). At day 16, bones subjected to 1 cycle were the only group with a mean percentage increase larger than that of the control bones. However, according to Figure 16, each bone subjected to 50 cycles had a percentage increase larger than the specific assigned control bone. This was only observed in that group and not in any of the others. Additionally, a variation in percentage length was prominent in the control group that displayed both the least and the largest percentage growth overall.

Bones subjected to 5 cycles and 50 cycles respectively decreased in growth rate after 11 days, whereas bones subjected to 1 and 10 cycles increased in growth rate during the same time period. The control bones exhibited a relatively linear behavior in growth rate after day 7.

Figure 17 is a comparison of the digital images taken of specimen #4 and #1 (Control and test for 1 cycle). From Figure 17, it can be seen how the growth plates changed during the trial.

By the end of the trial, the total mean percentage elongation of specimens subjected to 1, 5, 10, and 50 cycle was 180.3%, 173.9%, 175.7%, and 167.4% respectively. The control group exhibited an average percentage growth of 179.8%. The individual length measurements and percentage increases from trial 1 are presented in Table 2 and Table 3 of Appendix B.

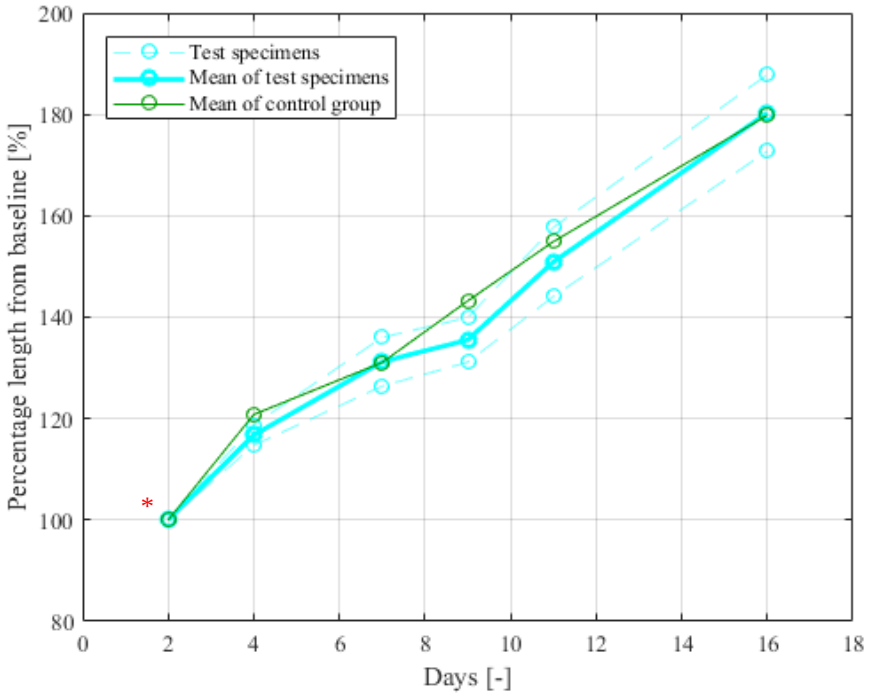

Figure 12: Percentage length for individual specimens in trial 1 subjected to 1 cycle of loading as measured over the course of 16 days. The bold line represents the calculated arithmetic mean of the test specimens. The green line represents the arithmetic mean of the control group. (* It is to be noted that the measurements from day zero in trial 1 were missing. As a result, day 2 served as baseline, denoted 100%)

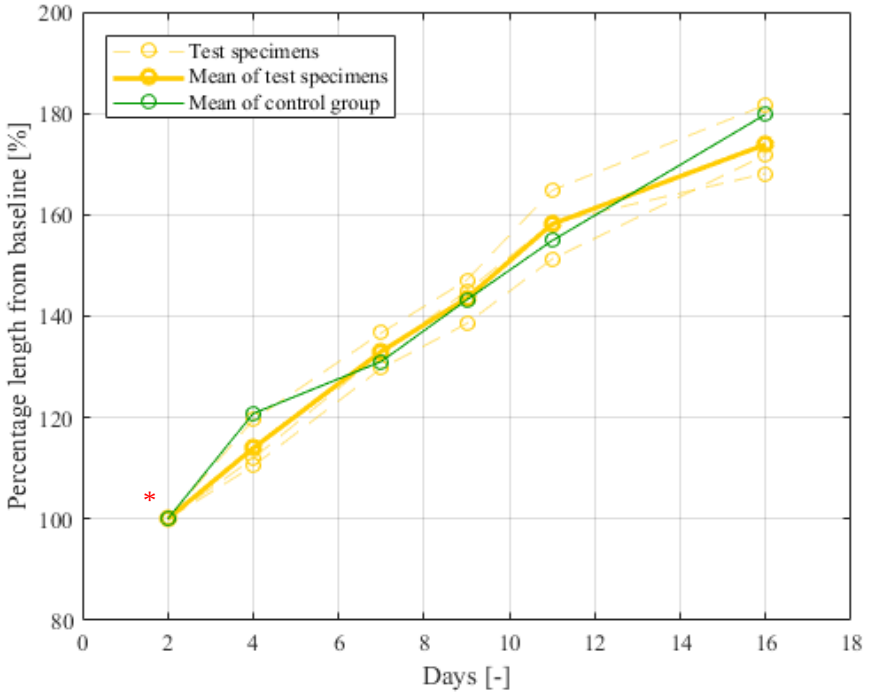

Figure 13: Percentage length for individual specimens in trial 1 subjected to 5 cycles of loading as measured over the course of 16 days. The bold line represents the calculated arithmetic mean of the test specimens. The green line represents the arithmetic mean of the control group. (* It is to be noted that the measurements from day zero in trial 1 were missing. As a result, day 2 served as baseline, denoted 100%)

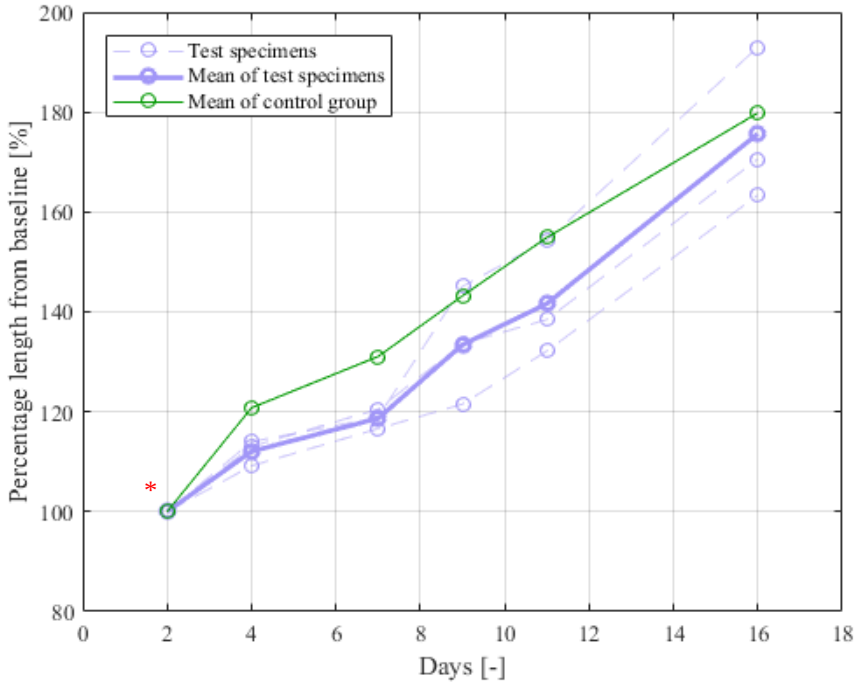

Figure 14: Percentage length for individual specimens in trial 1 subjected to 10 cycles of loading as measured over the course of 16 days. The bold line represents the calculated arithmetic mean of the test specimens. The green line represents the arithmetic mean of the control group. (* It is to be noted that the measurements from day zero in trial 1 were missing. As a result, day 2 served as baseline, denoted 100%)

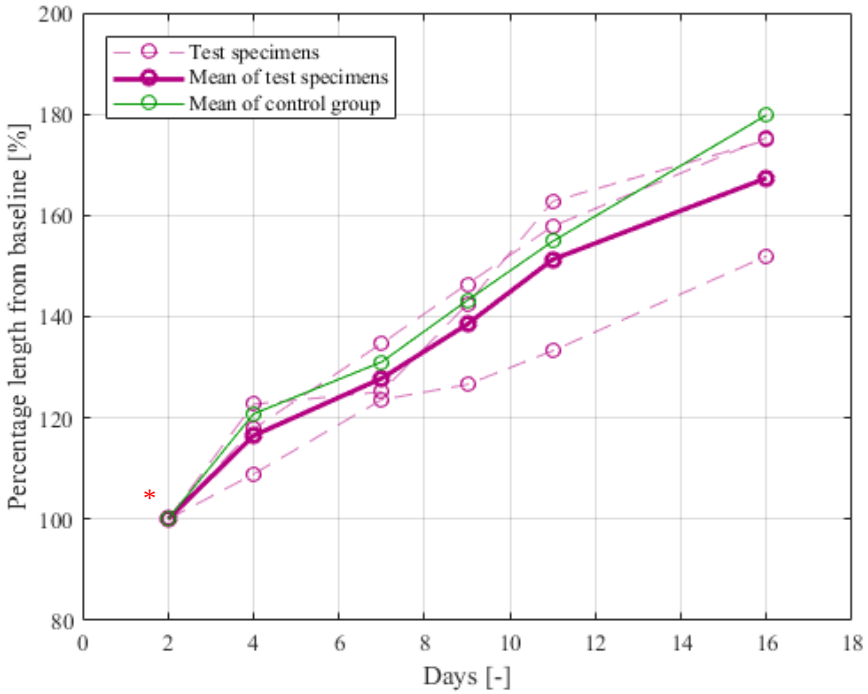

Figure 15: Percentage length for individual specimens in trial 1 subjected to 50 cycles of loading as measured over the course of 16 days. The bold line represents the calculated arithmetic mean of the test specimens. The green line represents the arithmetic mean of the control group. (* It is to be noted that the measurements from day zero in trial 1 were missing. As a result, day 2 served as baseline, denoted 100%)

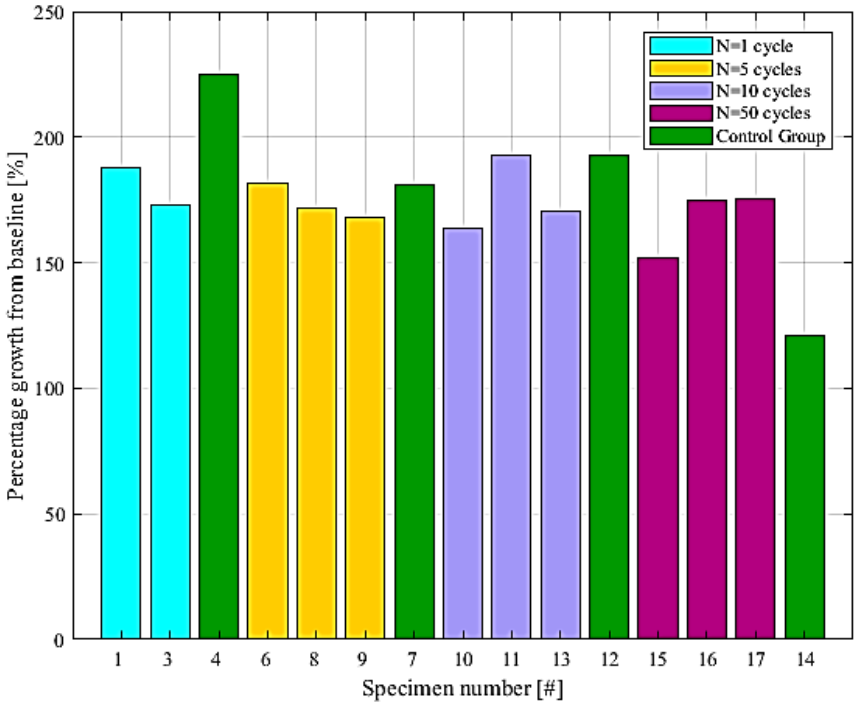

Figure 16: Graphical representation of percentage growth of each specimen in trial 1, at day 16

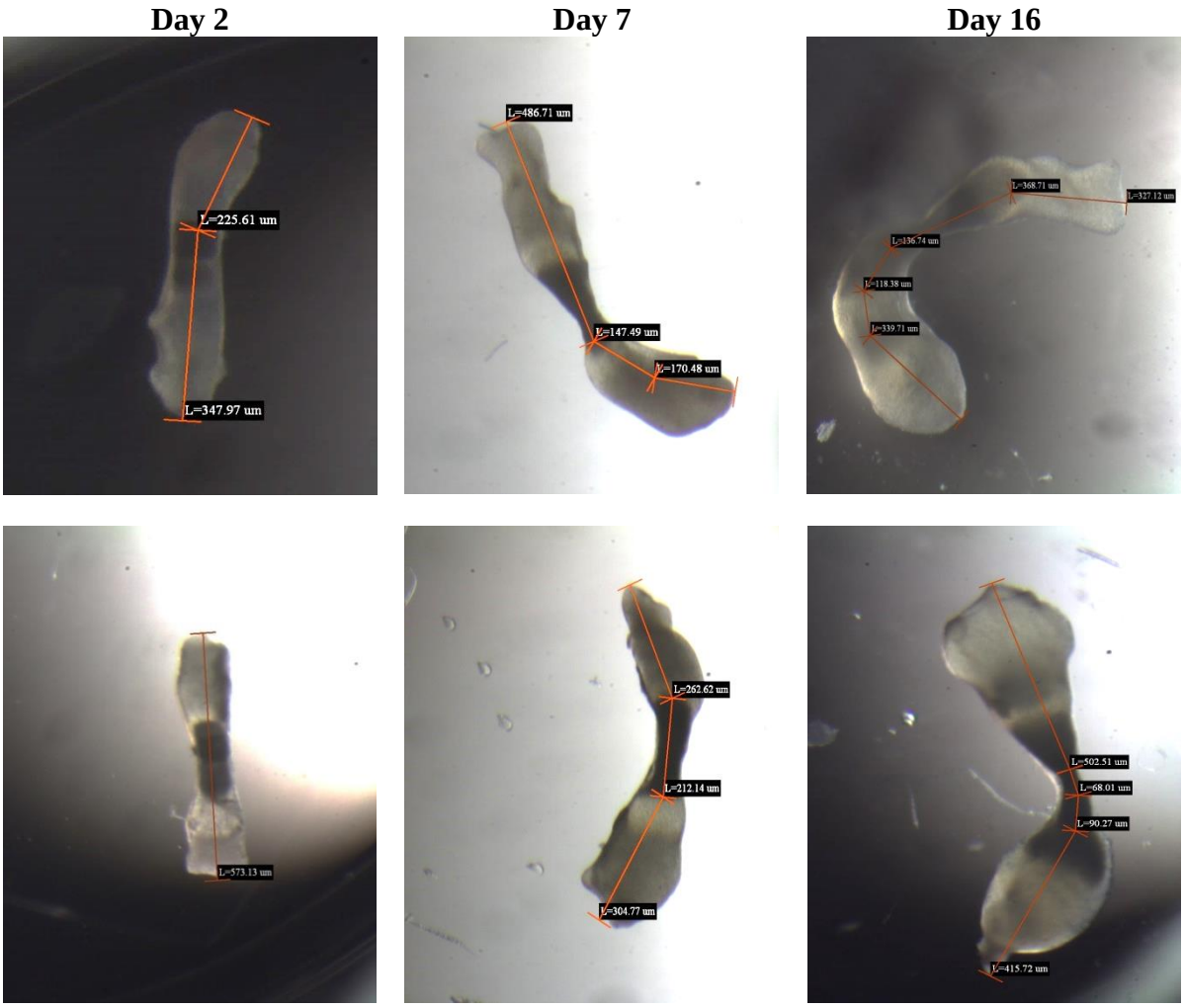

Figure 17: Length measurement and comparison of digital images of control specimen #4 (top row) and control specimen #1(bottom row) for trial 1. The darker areas are the mineralized bone while the lighter areas are the growth plates

5.1.2 Trial 2

The results of percentage length at each day of measurement from trial 2 were compiled and plotted in Figure 18 and Figure 19 and compared with the calculated mean of control bones. The percentage growth for each of the specimen after 16 days was plotted in the bar graph shown in Figure 20. Specimens #3 and #19 were damaged and broken during manual handling therefore were discarded from the analysis. Specimen #20 exhibited zero growth during the trial and it was therefore excluded from the analysis. The individual length measurement and percentage increase for trial 2 are presented in Table 4 and Table 5 of Appendix B.

At day 16, measured lengths revealed that the samples loaded with 5 cycles had the largest mean percentage increase. This trend was observed for that group throughout the whole trial. Bones subjected to 5 cycles and 50 cycles showed an increase in the growth rate between day 9 and day 14. After day 14, a slight decrease of the growth rate was observed in both test groups as well as the control group. Similar to trial 1, the control bones exhibit the largest variation.

At the end of the trial, specimens subjected to 5 cycles exhibited an average percentage growth of 190.9% while the specimens subjected to 50 cycles had an average percentage growth of 166.6%. The control bones grew 166.3% on average.

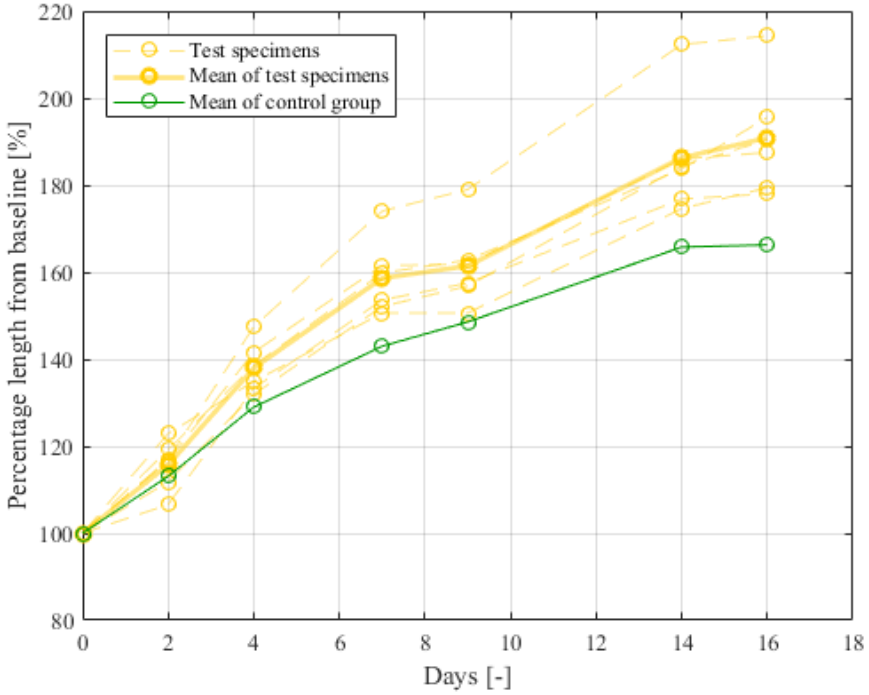

Figure 18: Percentage length for individual specimens in trial 2 subjected to 5 cycles of loading as measured over the course of 16 days. The bold line represents the calculated arithmetic mean of the test specimens. The green line represents the arithmetic mean of the control group

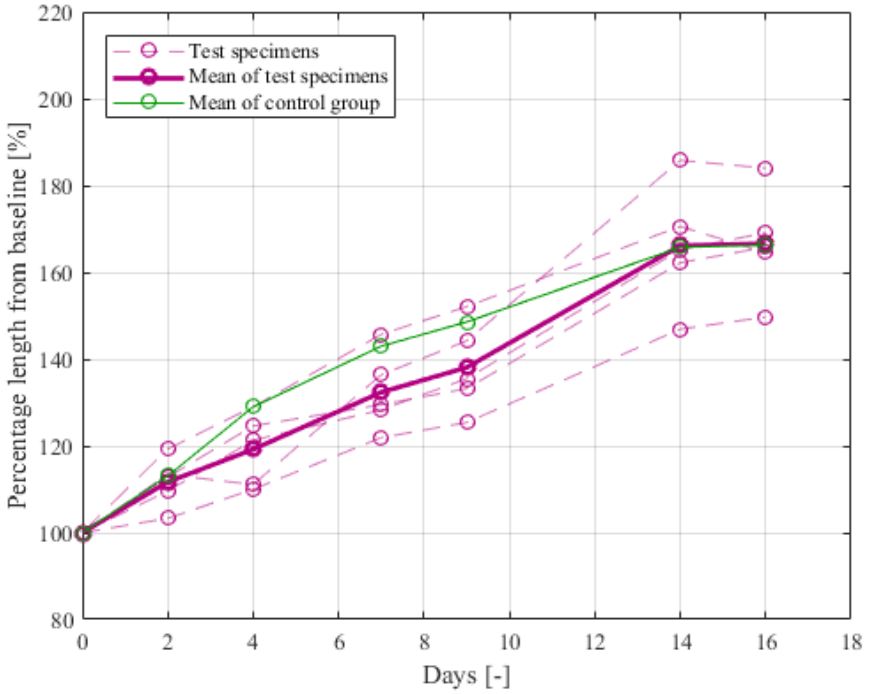

Figure 19: Percentage length for individual specimens in trial 2 subjected to 50 cycles of loading as measured over the course of 16 days. The bold line represents the calculated arithmetic mean of the test specimens. The green line represents the arithmetic mean of the control group

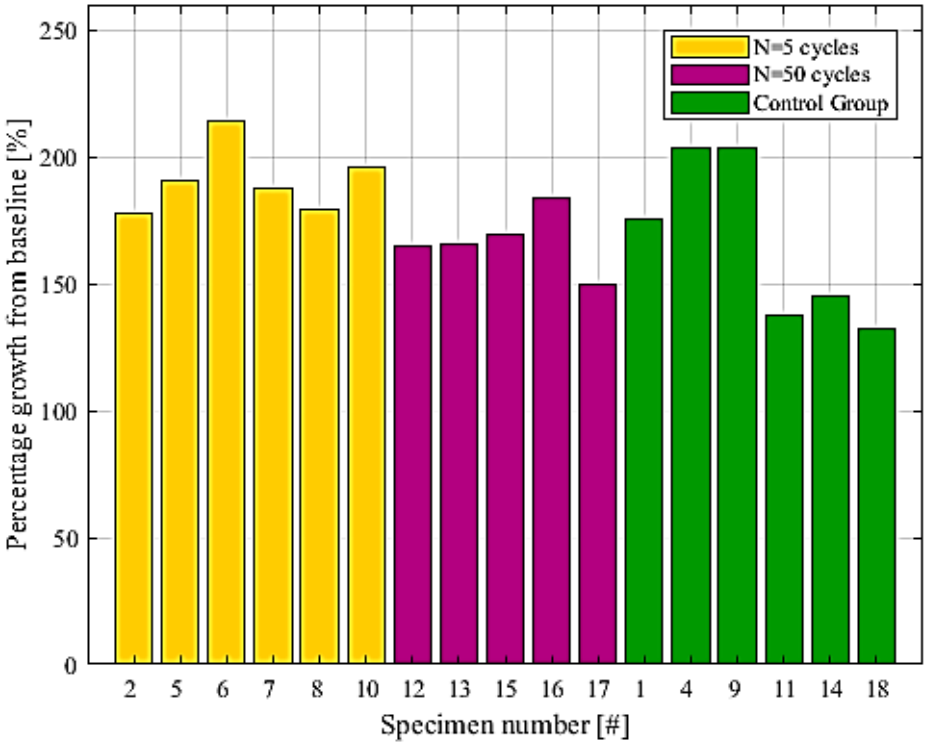

Figure 20: Graphical representation of percentage growth of each specimen in trial 2, at day 16

5.2 FEM Results

The results of the Finite Element analysis are presented below. Figure 21 and Figure 22 illustrate the temperature field at time 0 s and 1200 s, respectively for load case 1. It can be seen that the temperature gradually increased along the z-axis. The whole geometry had not reached the calcification temperature at the end of the simulation. Figure 23 and Figure 24 shows the displaced geometry at 100 s and 1200 s, respectively for load case 1. A total displacement of 0.96 mm was observed at the last time step of the simulation.

The results of load case 2 are shown in Figure 25-Figure 27. Following the temperature distribution as shown in Figure 25 and Figure 26, the geometry bent over time. It was observed that a greater elongation occurred closer to where the temperature was highest. Shown in the figures are the un-deformed wireframe and deformed geometry.

In both the cases studied, the higher stresses were closer to the lower boundary, where the fixed constraint was prescribed. The stresses throughout the geometry were relatively low, in the order of magnitude of kPa. The stress plots can be seen in Figure 30 and Figure 31 found in Appendix C.

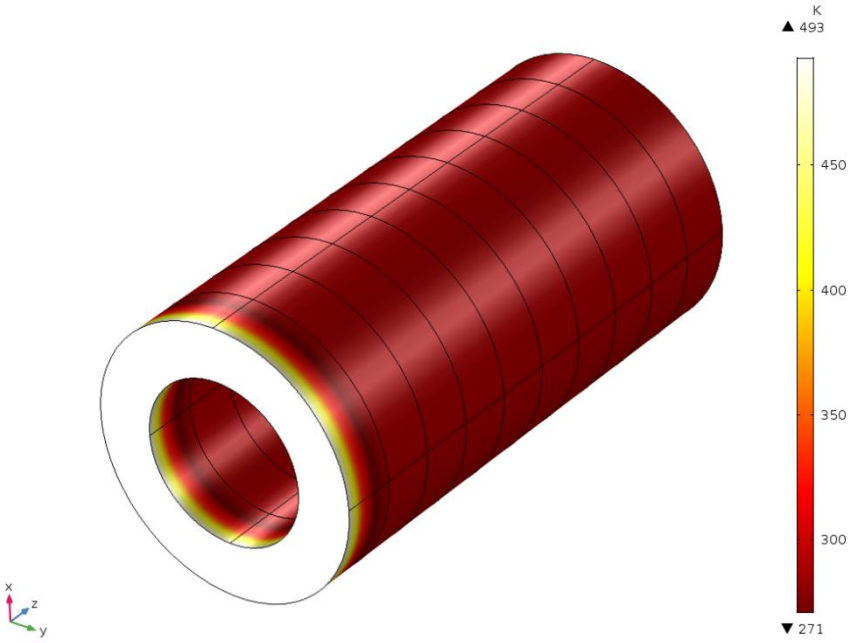

Figure 21: Temperature field in Kelvin at start for load case 1. 493.15 K represents the temperature at calcification

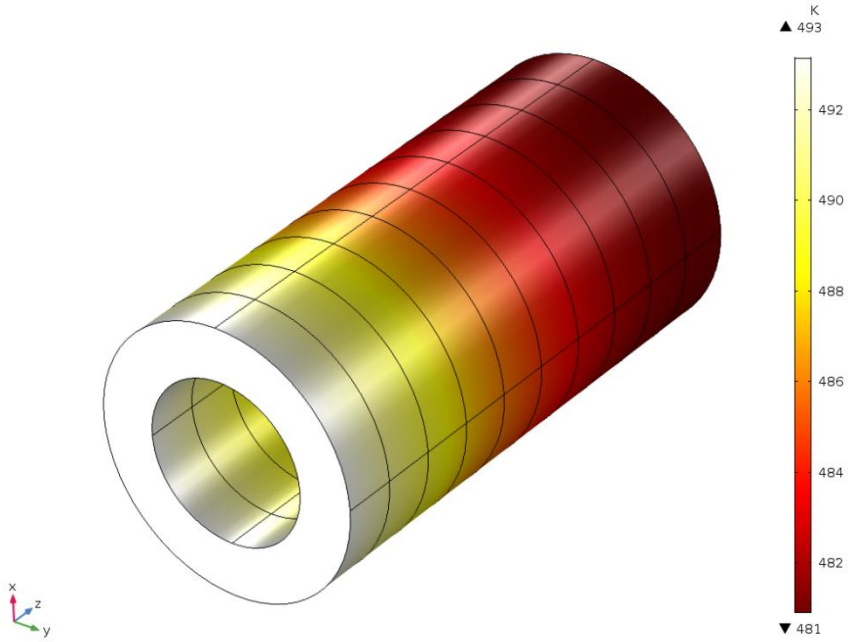

Figure 22: Temperature field in Kelvin at 1200s for load case 1. 493.15 K represents the temperature at calcification

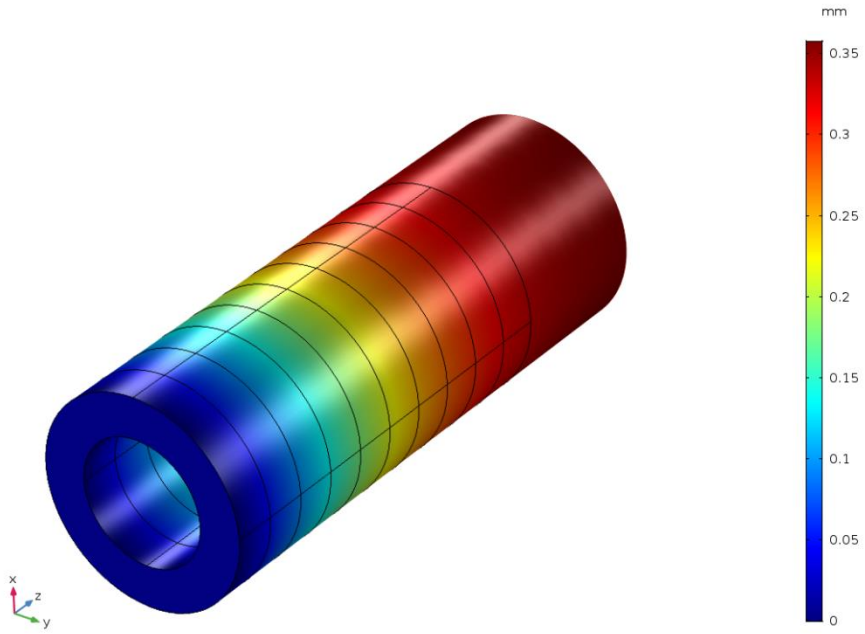

Figure 23: Total displacement at 100 s for load case 1

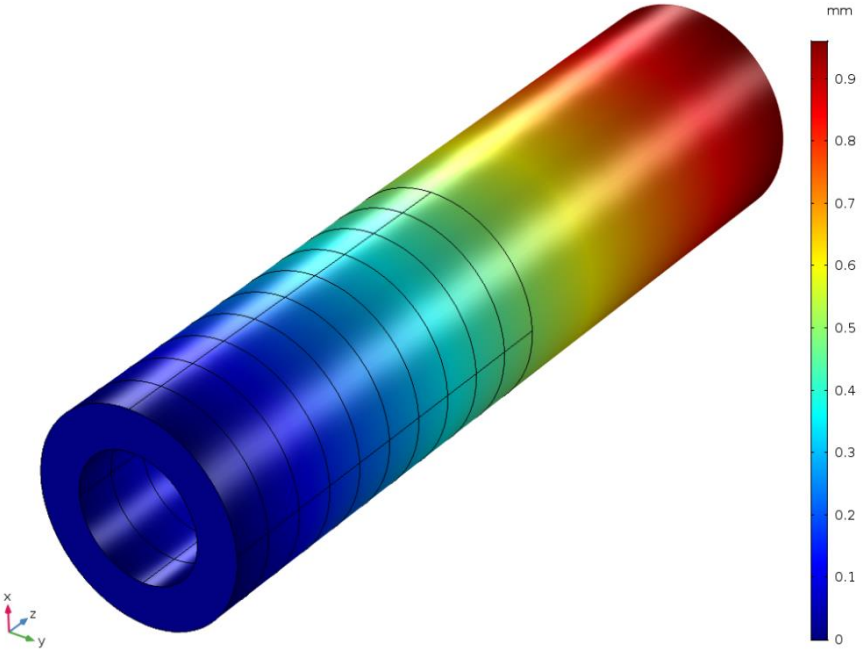

Figure 24: Total displacement at 1200 s load case 1

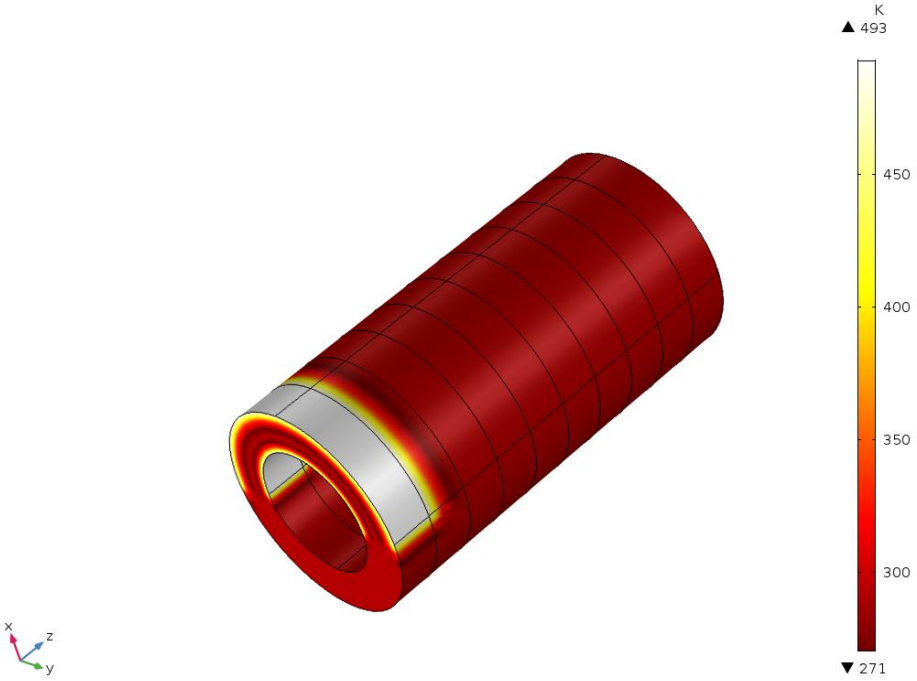

Figure 25: Temperature field in Kelvin at 0 s for load case 2. 493.15 K represents the temperature at calcification

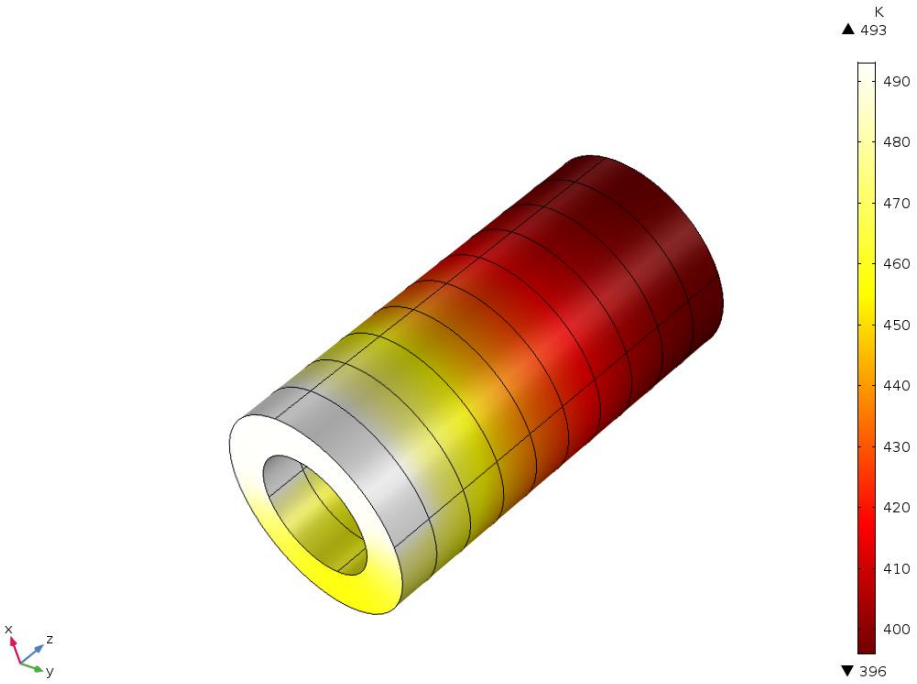

Figure 26: Temperature field in Kelvin at 400 s for load case 2. 493.15 K represents the temperature at calcification

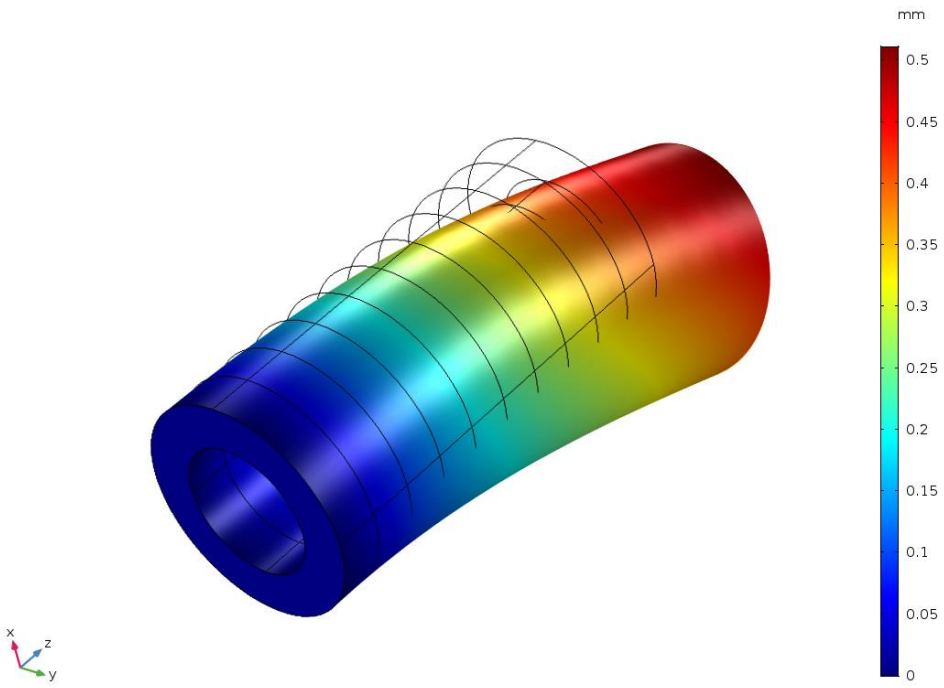

Figure 27: Total displacement at 100 s for load case 2

6 Discussion

The aim of the study was to observe how the number of cycles affects bone growth. The results from the both the first and second trials show that there is an effect that the loading cycles have on the bone growth. At day 11, it was observed that the specimens loaded with 5 cycles had a larger mean when compared to the mean value of the control bones. All other groups had a mean value lower than the control mean. This led to an additional study of the effect of loading with 5 and 50 cycles.

From the first trial results, it can also be observed how the average growth rates of the bones changed in comparison to the baseline throughout the course of 16 days. In the case of the specimen loaded with 5 and 50 cycles, it seems that the effect of the loading erodes after day 11 suggesting that despite a continued percentage increase, the effects of increasing the number of loading cycles do not have a lasting effect. A definitive conclusion could not be drawn from the results obtained from samples subjected to 10 loading cycles. The results from trial 1 also suggest that loading the bones once seems to cause a delayed response that eventually increases the mean percentage length. This is made evident by the control group having a larger growth increase up until day 4 compared to all the loaded groups. This is in agreement with Ménard et al. who investigated and compared the effects of both static and dynamic compressive loading in a series of experiments on rats. Their results showed that both static and dynamic compressive loading initially reduced the growth rate significantly compared to non-loaded specimens. However, continuing the experiment over a longer time period the results between the groups started to level out [16].

Trial 2 results exhibited a similar trend to the results obtained from trial 1. Specimens subjected to 50 cycles revealed almost the same total growth as the control group at the end of the trial. Similar to trial 1, the growth of the loaded specimens gave the impression of being delayed. Differences are however shown in the results from the specimens loaded with 5 cycles. After 16 days, the loaded bones exhibited a clear increase in mean growth compared to the control group. This increase was seen throughout the whole trial as opposed to trial 1 and the specimens subjected to 50 cycles in trial 2. Due to the small sample size, no statistical analysis was performed so it is not possible to determine if the increase is significant. However, analyzing each individual specimen in the group loaded with 5 cycles, an apparent trend was observed. Furthermore, trial 2 comprised of more specimens per group than trial 1, possibly making the results more reliable.

Due to the limited number of specimens, the peak load magnitude was calculated assuming an estimation of the cross sectional area of the bones which resulted in a peak load of 0.05 N. Since the magnitude was approximated, this could have affected the accuracy of the results. It is unclear whether a higher or lower magnitude would have yielded more distinct effects. A preferred method to select a suitable magnitude would have been to challenge a wide sample of bones with a broad range of magnitudes and observe their response.

These results could be a basis for supporting Frost's theory. Frost pointed out that a minimum effective strain threshold needs to be surpassed before bone adaptation would occur [10]. The theory assumed bone cells were in a way preconditioned with a set threshold to mechanical loading. There is a possibility that the bones tested never quite reach or surpass this threshold and that would explain why the effect of the loading in this study is short term for the majority of the tested groups. The cyclic loading induces some sort of growth response but not one to causes the osteocytes to adapt leading to a long term effect. In culture, rat metatarsal bones are known to grow up to three months after dissection [24]. It could be argued whether having a longer trial could show a different trend. If the bones are routinely exposed to an external load, they mechanosensors in the osteocytes may be able to accommodate this load. Furthermore, routinely adding an external load at the peaks may also lead to a continued accelerated percentage increase.

The accuracy of the results of the experiments was further affected by the testing equipment used. In order to load the bones in the longitudinal direction, a retrofitted holder was used. When placing the bones in the holder, it was theorized that the growth zone on one end of the bone was killed due to the

mechanical pressure of the holder. This decision was deliberate in order to apply pressure in the longitudinal direction on the growth zone on the other end of the bone. The control bones were however exposed to the exact same treatment except for the longitudinal loading, making the results comparable. The effect of removing the bones from the culture medium and exposing them to open air during each test is not clearly known and this may have also been a source for error. A more suitable experimental setup would have been one that ensured testing whilst the bones were still in the medium. Such a method also reduces the manual handling for the mechanical loading which is preferable since the bones are very small and delicate.

Some of the bones were bent as a result of the dissection as can be seen in Figure 17. A portion of these were purposely chosen to act as control bones so as to reduce possible damage from loading. However, from the results it can be seen that they still increased in length even though this bending could have affected the accuracy of the length measurements. Furthermore, the individual lengths of the specimens were measured by hand. A slight mismeasurement could have significantly affected the accuracy of the results. Due to the bent shape of some of the bones, the loading was not strictly longitudinal which most likely influenced the results. In addition, the retrofitted holder was not individually designed for each bone leading to difficulties in reproducing similar conditions in all tests. In order to continue investigate the effects of mechanical loading on immature metatarsals, the development of a different testing method is recommended.

The elongation obtained with load case 1 in the finite element simulations is comparable to the growth of the control group in the experiments. The computational model resulted in a relatively stress free structure with the exception of an area close to the fixed constraint, which is to be expected. Removing the constraint was however not an option since that would risk rigid body rotation. As seen in the experiments, bone growth is not strictly longitudinal. Load case 2 served to simulate a case in which a bone bends when growing. The added temperature on half of the geometry resulted in a higher temperature change in that area, thus increasing the displacement in accordance with general thermal expansion theory. The result is a bent geometry as shown in Figure 27.

The similarities in total elongation/growth show that the model could serve to simulate longitudinal growth. However, for it to predict the complete growth, further work is needed. The thermal properties, such as conductivity and specific heat, were arbitrarily chosen to obtain a suitable temperature field. Furthermore, for the purpose of this study, the longitudinal growth was of most importance. Therefore the expansion in all directions but the longitudinal was restricted, also reducing computational time. In order to create a thermal-structural coupling model capable of predicting all aspects of bone growth, the thermal and structural properties need to be investigated further.

The geometry of the growth zone was simplified to a hollow cylinder to reduce computational time. It would have been preferable to use an anatomically correct model. However, no CT-scans of the bones were performed and for the purpose of this study, the simplified geometry was considered sufficient.

In conclusion, the information obtained from the study reveals that bones are sensitive to mechanical loading even during the initial stages of development. There is a delayed growth response that results from compressive cycling loading of immature rat metatarsals. There may be a threshold for the number of cycles, below which compressive cyclic loading results in increased growth. Loading the metatarsals with 5 cycles seemed to have the most prominent effect over the course of 16 days. Further work is needed with suitable testing techniques to better investigate the effects of mechanical loading.

Bibliography

[1] S. Grässel and A. Aszódi, Cartilage: Volume 1: Physiology and development, 2016.

[2] G. Petje, R. Meizer, C. Radler, N. Aigner and F. Grill, "Deformity correction in children with hereditary hypophosphatemic rickets," *Clinical Orthopaedics and Related Research,* 2008.

[3] J. S. Khurana, Bone pathology, 2009.

[4] D. P. Lew and F. A. Waldvogel, "Osteomyelitis," *Lancet,* 2004.

[5] I. Villemure and I. A. F. Stokes, *Growth plate mechanics and mechanobiology. A survey of present understanding,* 2009.

[6] "SYBIL," European Community's Seventh Framework Programme , 2013. [Online]. Available: http://www.sybil-fp7.eu/Growth%20plate. [Accessed 30 05 2018].

[7] "Obgyn Key," 18 07 2016. [Online]. Available: https://obgynkey.com/growth-plate-anatomy/. [Accessed 30 05 2018].

[8] J. Wolff, "Das Gesetz der Transformation der Knochen," *Deutsche Medizinische Wochenschrift,* 1893.

[9] D. W. Thompson, "On form and mechanical efficiency BT - On Growth and Form," in *On Growth and Form,* 1961.

[10] H. M. Frost, "Biomechanical control of knee alignment: some insights from a new paradigm.," *Clinical orthopaedics and related research,* 1997.

[11] M. Lisková and J. Hert, "Reaction of bone to mechanical stimuli. 2. Periosteal and endosteal reaction of tibial diaphysis in rabbit to intermittent loading.," *Folia morphologica,* 1971.

[12] L. E. Lanyon and C. T. Rubin, *Static vs dynamic loads as an influence on bone remodelling,* 1984.

[13] C. T. Rubin and K. J. McLeod, "Promotion of bony ingrowth by frequency-specific, low-amplitude mechanical strain.," *Clinical orthopaedics and related research,* 1994.

[14] C. H. Turner, "Three rules for bone adaptation to mechanical stimuli," *Bone,* 1998.

[15] I. A. Stokes, P. L. Mente, J. C. Iatridis, C. E. Farnum and D. D. Aronsson, "Enlargement of growth plate chondrocytes modulated by sustained mechanical loading," *Journal of Bone and Joint Surgery - Series A,* 2002.

[16] A. L. Ménard, G. Grimard, I. Londono, F. Beaudry, P. Vachon, F. Moldovan and I. Villemure, "Bone growth resumption following in vivo static and dynamic compression removals on rats," *Bone,* 2015.

[17] R. L. De Souza, M. Matsuura, F. Eckstein, S. C. Rawlinson, L. E. Lanyon and A. A. Pitsillides, "Non-invasive axial loading of mouse tibiae increases cortical bone formation and modifies trabecular organization: A new model to study cortical and cancellous compartments in a single loaded element," *Bone*, 2005.

[18] D. Sriram, A. Jones, I. Alatli-Burt and M. A. Darendeliler, "Effects of mechanical stimuli on adaptive remodeling of condylar cartilage," *Journal of Dental Research*, 2009.

[19] M. Thibault, A. R. Poole and M. D. Buschmann, "Cyclic compression of cartilage/bone explants in vitro leads to physical weakening, mechanical breakdown of collagen and release of matrix fragments," *Journal of Orthopaedic Research*, 2002.

[20] E. Novitskaya, S. Lee, V. A. Lubarda and J. McKittrick, "Initial anisotropy in demineralized bovine cortical bone in compressive cyclic loading-unloading," *Materials Science and Engineering C*, 2013.

[21] M. Ueki, N. Tanaka, K. Tanimoto, C. Nishio, K. Honda, Y. Y. Lin, Y. Tanne, S. Ohkuma, T. Kamiya, E. Tanaka and K. Tanne, "The effect of mechanical loading on the metabolism of growth plate chondrocytes," *Annals of Biomedical Engineering*, 2008.

[22] E. Maeda, M. Nakagaki, K. Ichikawa, K. Nagayama and T. Matsumoto, "Effects of cyclic compression on the mechanical properties and calcification process of immature chick bone tissue in culture," *Bone Reports*, 2017.

[23] J. J. Vaca-González, M. Moncayo-Donoso, J. M. Guevara, Y. Hata, S. J. Shefelbine and D. A. Garzón-Alvarado, "Mechanobiological modeling of endochondral ossification: an experimental and computational analysis," *Biomechanics and Modeling in Mechanobiology*, vol. 17, no. 3, pp. 853-875, 2018.

[24] F. Zaman, Interviewee, [Interview]. 11 04 2018.

Appendix A

Examples of cyclic loading of specimen in ADMET Materials Testing Machine with data analyzed with MTESTQuattro

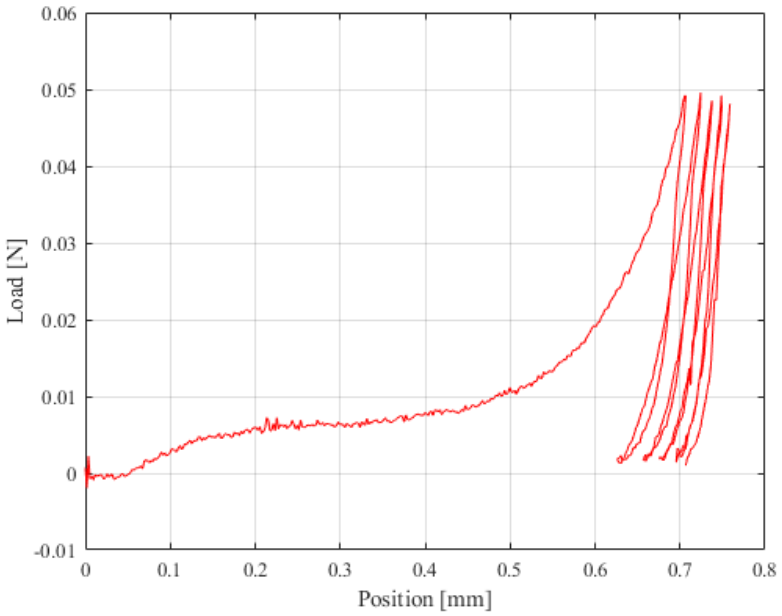

Figure 28: Loading with 5cycles

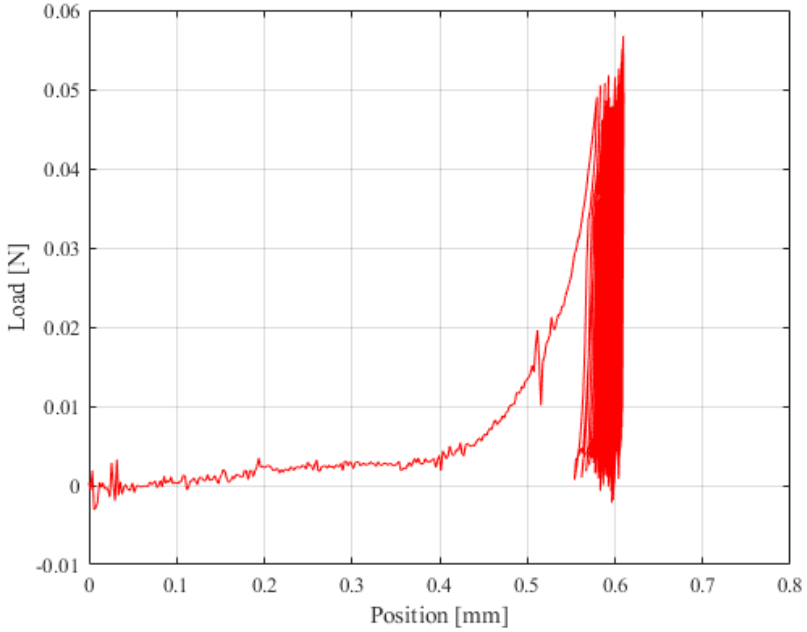

Figure 29: Loading with 50 cycles

Appendix B

This appendix shows the total length and percentage length of each specimen for the various measurement days in trial 1 and trial 2

Table 2: Total length of each specimen in trial 1, for each day of measurement

Specimen #	**Day 2** (μm)	**Day 4** (μm)	**Day 7** (μm)	**Day 9** (μm)	**Day 11** (μm)	**Day 16** (μm)
1	573.1	680.7	779.5	802.0	903.8	1076.5
2	566.2	762.5	829.0	886.9	1072.2	1239.4
3	477.8	548.3	604.0	626.5	688.5	825.5
4	573.6	725.7	804.7	900.2	1029.8	1290.7
5	307.8	350.0	515.5	549.6	580.0	668.0
6	669.3	800.1	915.0	984.5	1103.1	1215.9
7	803.1	990.6	1078.6	1232.0	1275.2	1452.7
8	647.2	714.7	839.5	896.6	978.8	1112.0
9	634.8	710.5	842.4	920.3	1005.6	1067.5
10	605.4	660.9	705.9	735.8	800.0	989.1
11	603.4	687.9	717.4	875.5	931.2	1164.5
12	558.5	700.2	768.8	832.2	913.7	1075.5
13	612.0	691.8	737.5	817.9	847.4	1044.1
14	564.7	609.7	632.5	640.8	664.5	682.2
15	637.6	694.5	788.2	807.2	849.8	969.0
16	588.0	721.5	735.9	837.7	957.2	1028.0
17	669.8	789.3	902.4	980.9	1057.3	1174.5

Table 3: Percentage length from day 2 of each specimen in trial 1, for each day of measurement

Specimen #	**Day 2** (%)	**Day 4** (%)	**Day 7** (%)	**Day 9** (%)	**Day 11** (%)	**Day 16** (%)
1	100	118.8	136.0	139.9	157.7	187.8
2	100	134.7	146.4	156.6	189.4	218.9
3	100	114.7	126.4	131.1	144.1	172.8
4	100	126.5	140.3	156.9	179.5	225.0
5	100	113.7	167.5	178.5	188.4	217.0
6	100	119.5	136.7	147.1	164.8	181.7
7	100	123.4	134.3	153.4	158.8	180.9
8	100	110.4	129.7	138.5	151.2	171.8
9	100	111.9	132.7	145.0	158.4	168.2
10	100	109.2	116.6	121.5	132.2	163.4
11	100	114.0	118.9	145.1	154.3	193.0
12	100	125.4	137.7	149.0	163.6	192.6
13	100	113.0	120.5	133.6	138.5	170.6
14	100	108.0	112.0	113.5	117.7	120.8
15	100	108.9	123.6	126.6	133.3	152.0
16	100	122.7	125.2	142.5	162.8	174.8
17	100	117.8	134.7	146.5	157.9	175.4

Table 4: Total length of each specimen in trial 2, for each day of measurement

Specimen #	**Day 0** (µm)	**Day 2** (µm)	**Day 4** (µm)	**Day 7** (µm)	**Day 9** (µm)	**Day 14** (µm)	**Day 16** (µm)
1	650.8	676.4	809.8	882.4	998.4	1141.9	1140.0
2	696.5	742.1	928.5	1070.0	1096.9	1231.4	1239.6
3	718.3	356.6	-	-	-	-	
4	611.9	934.2	1009.3	1063.5	1104.8	1256.7	1247.1
5	614.0	686.4	810.1	933.9	962.5	1131.9	1169.3
6	586.8	686.4	865.5	1021.3	1050.2	1246.0	1257.4
7	599.3	699.6	848.7	968.0	969.8	1115.0	1123.8
8	644.7	792.4	869.8	970.9	970.9	1125.6	1156.5
9	722.5	781.7	1025.1	1307.9	1333.5	1470.7	1469.3
10	662.2	789.3	918.0	1057.9	1077.9	1216.5	1295.5
11	660.9	695.8	761.0	806.4	766.7	852.6	911.7
12	609.8	727.5	786.9	888.2	927.8	1040.3	1003.0
13	670.6	756.3	835.3	868.5	892.9	1087.8	1111.6
14	575.6	614.4	669.5	713.4	764.6	843.8	837.2
15	663.7	727.4	805.1	851.5	899.3	1096.7	1122.0
16	689.3	781.8	766.0	939.9	993.9	1280.4	1268.4
17	616.3	636.7	678.0	751.3	772.6	905.1	922.3
18	637.0	647.7	708.4	774.4	789.8	857.6	840.7
19	703.5	928.2	1046.5	1051.6	1212.3	1250.4	1259.5
20	702.6	703.6	701.0	711.9	684.5	689.4	661.6

Table 5: Percentage length from day 0 of each specimen in trial 2, for each day of measurement

Specimen #	**Day 0** (%)	**Day 2** (%)	**Day 4** (%)	**Day 7** (%)	**Day 9** (%)	**Day 14** (%)	**Day 16** (%)
1	100	103.9	124.4	135.6	153.4	175.5	175.2
2	100	106.6	133.3	153.6	157.5	176.8	178.0
3	100	49.6	-	-	-	-	
4	100	152.7	164.9	173.8	180.6	205.4	203.8
5	100	111.8	131.9	152.1	156.8	184.3	190.4
6	100	117.0	147.5	174.0	179.0	212.3	214.3
7	100	116.7	141.6	161.5	161.8	186.0	187.5
8	100	122.9	134.9	150.6	150.6	174.6	179.4
9	100	108.2	141.9	181.0	184.6	203.5	203.3
10	100	119.2	138.6	159.8	162.8	183.7	195.6
11	100	105.3	115.2	122.0	116.0	129.0	137.9
12	100	119.3	129.0	145.7	152.1	170.6	164.5
13	100	112.8	124.6	129.5	133.2	162.2	165.8
14	100	106.7	116.3	123.9	132.8	146.6	145.4
15	100	109.6	121.3	128.3	135.5	165.2	169.1
16	100	113.4	111.1	136.4	144.2	185.8	184.0
17	100	103.3	110.0	121.9	125.4	146.9	149.7
18	100	101.7	111.2	121.6	124.0	134.6	132.0
19	100	131.9	148.8	149.5	172.3	177.7	179.0
20	100	100.2	99.8	101.3	97.4	98.1	94.2

Appendix C

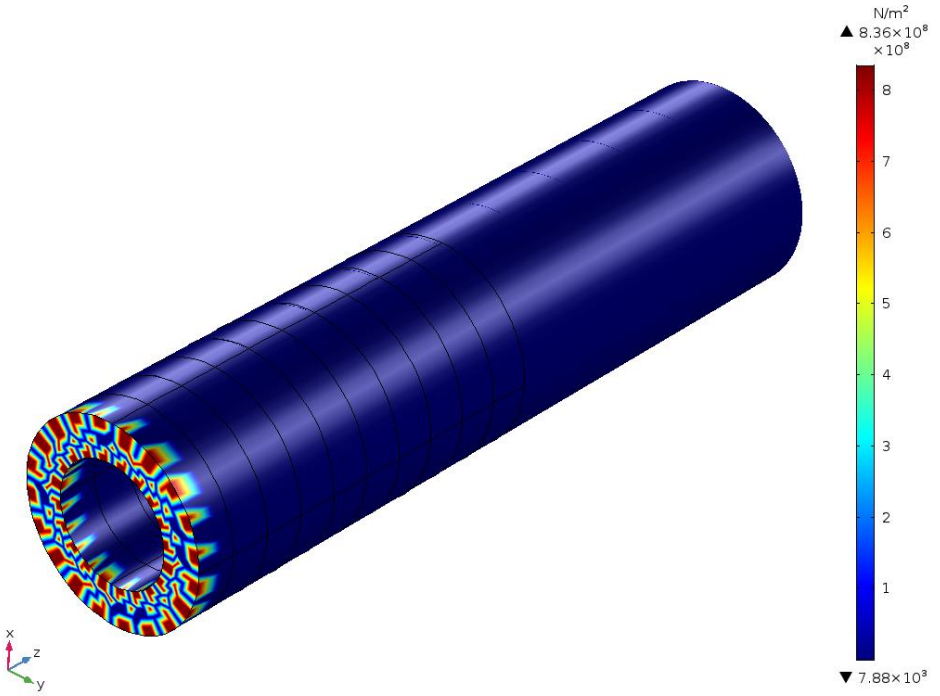

Figure 30: Stress plot at 1200 s for load case 1

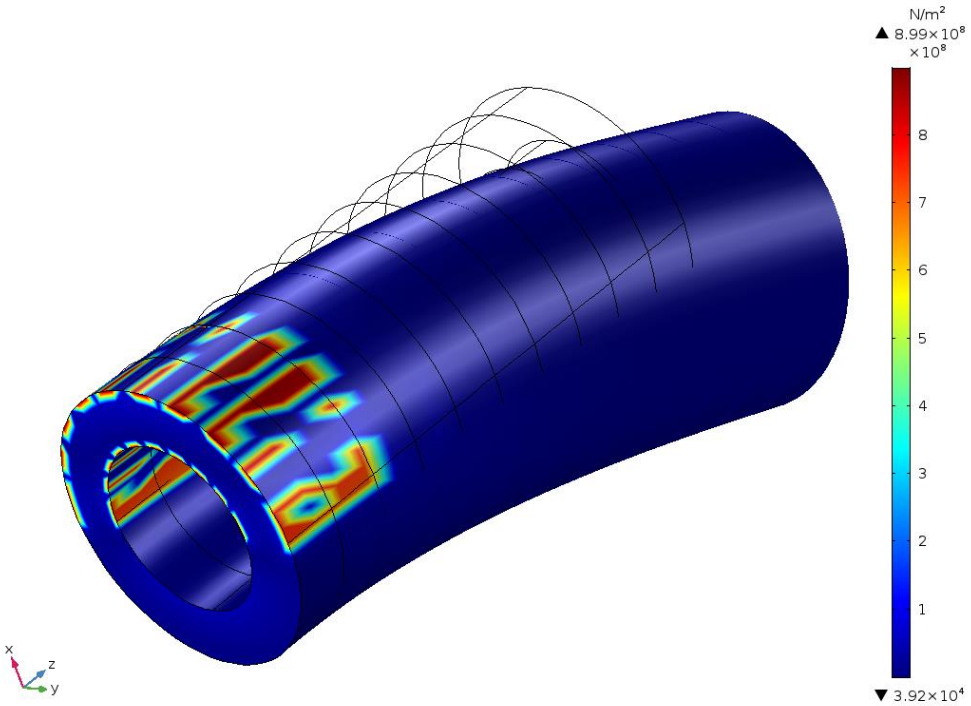

Figure 31: Stress plot at 100 s for load case 2